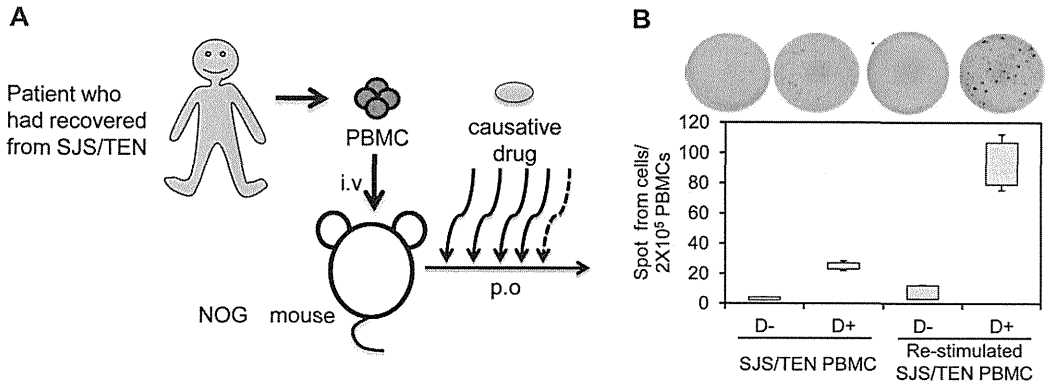

FIG 1. Development of SJS/TEN model mice by using PBMCs of patients who had recovered from SJS/TEN. **A,** Scheme of model mice development. PBMCs were obtained from patients who had recovered from SJS/TEN. These PBMCs (2×10^6) were injected intravenously into NOG mice, followed by oral administration of the causative drugs. **B,** Causative drug–specific cells were detected by using the human IFN-γ ELISpot. When the causative drug was added to cultured PBMCs of patients who had recovered from SJS/TEN (patient 2), causative drug–specific lymphocytes were detected (30 spots per 2×10^5 cells). After 2 stimulations of the causative drug (restimulation), the number of drug-specific lymphocytes increased (90 spots per 2×10^5 cells). Samples from patients 1 to 6 with SJS/TEN were analyzed, and representative data (patient 2) are shown. *i.v.*, Intravenous; *p.o.*, by mouth.

Measurement of human granulysin and human/mouse sFasL

Human granulysin and human/mouse sFasL in supernatants of PBMCs or sera from SJS/TEN model mice were measured by using ELISA. Human granulysin ELISA (BML, Tokyo, Japan) was performed as previously reported.[11] Human/mouse sFasL levels were measured by using an ELISA kit from R&D Systems (Minneapolis, Minn).

SJS/TEN mouse model using patients' PBMCs and skin

Full-thickness skin grafts from healthy control subjects or patients who had recovered from SJS/TEN or an ODSR were transplanted onto the NOG mice. After skin engraftment (approximately 12 days after transplantation), causative drug–stimulated PBMCs (2×10^6) from the same patient were injected intravenously into these mice, followed by oral administration of the causative drug. Changes in skin graft appearance, such as darkening, were observed. The skin grafts were investigated histopathologically.

RESULTS

Development of SJS/TEN mouse model using PBMCs from patients who had recovered from SJS/TEN

To develop the SJS/TEN mouse model, we used PBMCs from patients who had recovered from SJS/TEN. The PBMCs were injected intravenously into immunocompromised mice, followed by oral administration of the causative drug (Fig 1, *A*). There are several reports on the existence of drug-specific lymphocytes in patients who had recovered from drug allergies, and these lymphocytes were restimulated by the causative drug *in vitro*.[17,18] Therefore if lymphocytes that specifically reacted to the drug remained in the peripheral blood, these lymphocytes would be restimulated by the causative drug, and identical immunologic reactions to those of patients with active SJS/TEN would occur in the mice.

First, we confirmed the presence of causative drug–specific lymphocytes in peripheral blood. ELISpot analysis of human IFN-γ was conducted to detect antigen-specific human cells. When the causative drug was added to cultured PBMCs from patients who had recovered from SJS/TEN, causative drug–specific lymphocytes were detected (Fig 1, *B*). After *in vitro* restimulation of the causative drug, the number of drug-specific lymphocytes increased. To exclude the possibility of *in vitro* priming of naive T cells, we performed the ELISpot assay using PBMCs of naive healthy volunteers who had never experienced cutaneous adverse drug reactions. We stimulated the PBMCs of healthy volunteers (n = 4) with amoxicillin, one of the causative drugs in our study, and restimulated them after 5 days. In ELISpot data we were unable to detect drug-specific T cells, even on restimulation (see Fig E1 in this article's Online Repository at www.jacionline.org). Either a breakdown product or a drug metabolite might be the drug form that is responsible for drug reactions that are presumed to be immunologic in nature. On the other hand, in our experiments the addition of native drugs to PBMCs induced the activation of drug-specific lymphocytes, indicating that a breakdown product of the drug might be recognized as an antigen *in vitro*. These data reconfirm that even after resolution of SJS/TEN, drug-specific lymphocytes still circulate, as previously reported.[18]

We used NOG mice, which lack T cells, B cells, and natural killer (NK) cells, as immunocompromised mice.[19] NOG mice are characterized by tolerance to human cells, which enables humanized mice to be established.[20] However, when human cells are applied to NOG mice, GVHRs can occur because engrafted human immune cells attack mouse tissues.[21] The NOG mice showed GVHD symptoms at 46.3 ± 14.3 days after intravenous transplantation of 2.5×10^6 PBMCs.[21] Indeed, at 40 days after human PBMCs were injected intravenously into the NOG mice, weight loss, skin erosion, and diarrhea were noticed as symptoms of GVHRs in our experiments. The skin lesions of patients with GVHRs were quite similar to those of patients with SJS/TEN. Skin erosion and hair loss were observed clinically, and epithelial cell death and epidermal detachment were observed histologically. In addition, human $CD45^+$ cells were detected in mouse peripheral blood at 20 days after PBMC injection (see Fig E2 in this article's Online Repository at www.jacionline.org), showing that activation of injected human cells had occurred in the NOG mice.

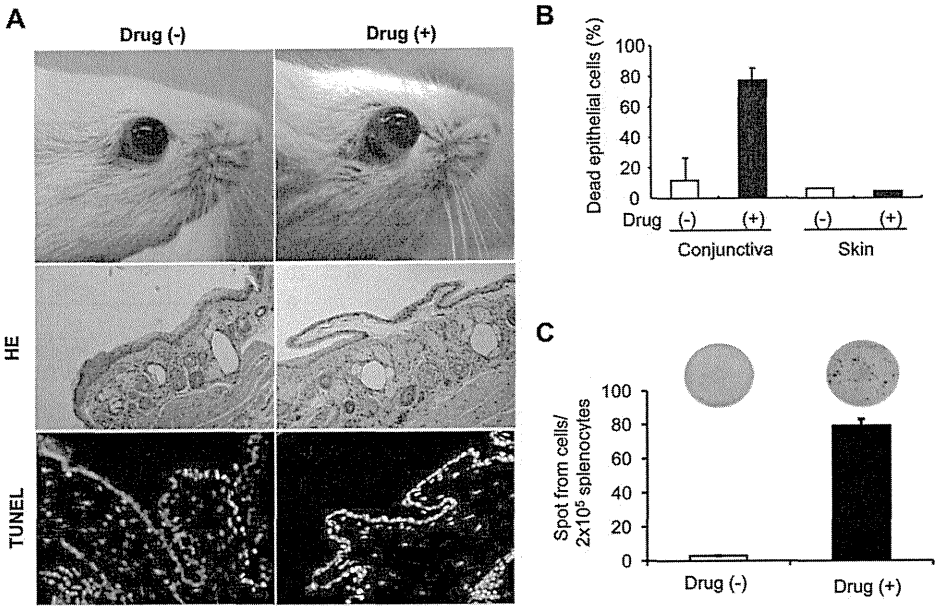

FIG 2. PBMCs from patients with SJS/TEN and causative drug–induced ocular manifestations similar to those of SJS/TEN in NOG mice. **A** and **B,** At 12 days after PBMC injection and causative drug intake, significant conjunctival congestion and conjunctival chemosis are noticed. The PBMC-injected mice without causative drug intake showed no such symptoms. Histologic analysis showed marked edema of the conjunctival subepithelia in the SJS/TEN-PBMC$^+$drug$^+$ mice. The TUNEL assay detected numerous dead epithelial cells in the SJS/TEN-PBMC$^+$drug$^+$ mice (78% of cells) but not in the SJS/TEN-PBMCs$^+$drug$^-$ mice (5% of cells). There was no increase in keratinocyte death in the skin in either group. *HE,* Hematoxylin and eosin. **C,** Human IFN-γ ELISpot with mice splenocytes was performed to confirm that causative drug–specific immune reaction occurred in those mice. At 12 days after PBMC injection, the number of causative drug–specific lymphocytes in the SJS/TEN-PBMC$^+$drug$^+$ mice was significantly increased compared with that of the SJS/TEN-PBMC$^+$drug$^-$ mice. Samples from patients 1, 2, 4, and 5 with SJS/TEN and patient 1 with an ODSR were used, and representative data (patient 2) are shown.

In contrast, within 20 days after PBMC injection, no GVHR symptoms appeared (n = 5). Therefore to distinguish clearly between GVHRs and SJS/TEN reactions, we examined mouse model experiments up to 14 days after PBMC administration.

At 12 days after PBMC injection and causative drug intake, marked conjunctival congestion and conjunctival chemosis were noticed, whereas PBMC-injected mice without causative drug intake showed no such symptoms (Fig 2, *A*). Histologic analysis showed marked edema of the conjunctival subepithelia and vasodilatation in mice receiving PBMCs and causative drug administration (SJS/TEN-PBMC$^+$drug$^+$ mice). We made 20 model mice, all of which showed similar manifestations. Furthermore, the TUNEL assay found numerous dead epithelial cells in the SJS/TEN-PBMC$^+$drug$^+$ mice (78% of cells; Fig 2, *B*) but not in the PBMC-injected, non–drug-administered (SJS/TEN-PBMC$^+$drug$^-$) mice (5% of cells). Unexpectedly, there were no skin manifestations in either group and no difference in percentages of dead keratinocytes between the groups. At 40 days after PBMC injection, weight loss, skin erosion, hair loss, and diarrhea were noticed. Prominent epithelial cell death was observed histologically (see Fig E3 in this article's Online Repository at www.jacionline.org). These data were virtually identical to those of the GVHD model.

To analyze the occurrence mechanism of SJS/TEN in the model mice, we investigated various conditions that might elicit ocular manifestations similar to those of patients with SJS/TEN (Table I). We observed conjunctival congestion and conjunctival chemosis in our model mice.

TABLE I. Occurrence of ocular manifestations in NOG mice in various conditions

Injected cells	Causative drug intake	Ocular manifestations
PBMCs from patients with SJS/TEN	+	+ (Day 12)
PBMCs from patients with SJS/TEN	−	−
Restimulated PBMCs from patients with SJS/TEN	+	+ (Day 6)
PBMC–depleted CD4$^+$ cells from patients with TEN	+	+ (Day 14)
PBMC–depleted CD4$^+$ cells from patients with TEN	+	−
PBMCs from patients with ODSRs	+	−
PBMCs from patients with ODSRs	−	−
Healthy control PBMCs	+	−
Healthy control PBMCs	−	−
None	+	−

Samples from patients 1 and 2 with SJS/TEN and patient 1 with an ODSR were analyzed, and representative data (patient 2 with SJS/TEN and patient 1 with an ODSR) are shown.

Causative drug intake alone did not induce ocular manifestations in the NOG mice. Healthy control PBMCs and acetaminophen, amoxicillin, or phenytoin, which were the causative drugs in the patients with SJS/TEN described in this article, also did not induce ocular manifestations. Importantly, PBMCs from patients who recovered from ODSRs (ie, nonsevere drug-induced skin reactions) and causative drug intake did not elicit ocular

manifestations. However, we were able to find drug-specific T cells in the spleens of NOG mice after ODSR PBMC transfer and orally administered causative drug by using the same ELISpot assay (see Fig E4 in this article's Online Repository at www.jacionline.org). These data showed the ocular manifestations to be a phenomenon specific to PBMCs from patients with SJS/TEN. In addition, causative drug–restimulated PBMCs from patients with SJS/TEN accelerated the onset of ocular manifestations. $CD4^+$ or $CD8^+$ T lymphocytes were depleted from the PBMCs to identify which lymphocyte subtype is critical in inducing ocular manifestations. $CD4^+$ T lymphocyte–depleted PBMCs from patients with SJS/TEN were able to induce ocular manifestations, whereas $CD8^+$ T lymphocyte–depleted PBMCs from patients with SJS/TEN were not (see Fig E5 in this article's Online Repository at www.jacionline.org).

These data demonstrate that we have succeeded in establishing model mice showing ocular manifestations (ie, SJS/TEN model mice). In addition, the ocular manifestations similar to those of patients with SJS/TEN in NOG mice were found to be dependent on the causative drug–specific lymphocytes of patients with SJS/TEN, and $CD8^+$ T cells are essential to this phenomenon.

Soluble factors, such as granulysin, were not mediators of conjunctival cell death in the SJS/TEN mouse model

In our novel SJS/TEN mouse model, there were almost no infiltrating human cells (human $CD45^+$ cells) in the conjunctiva, whereas numerous human cells were detected in the conjunctiva of the mice with GVHRs (see Fig E6 in this article's Online Repository at www.jacionline.org). Therefore it might be that conjunctival cell death is partially induced by soluble factors in addition to direct lymphocyte-epithelium interaction. As mentioned above, we and others have shown that granulysin might contribute to SJS/TEN occurrence. We examined granulysin levels in the supernatants of causative drug–stimulated PBMCs. Causative drug–stimulated PBMCs from patients with SJS/TEN secreted granulysin at levels less than (0.2 ± 0.3 ng/mL) than the serum levels of patients with acute-phase SJS/TEN (24.8 ± 21.2 ng/mL) and those of healthy control subjects (1.6 ± 0.6 ng/mL).[11] In addition, granulysin immunohistostaining in the conjunctiva of SJS/TEN model mice and in grafted skin from patients with SJS-TEN showed almost no granulysin expression in these tissues (data not shown). Furthermore, human granulysin and sFasL levels in the sera of mice were measured at days 8 and 12. Serum levels of human granulysin and sFasL were undetectable at these time points. Although ELISA for murine granulysin was not available, we measured murine sFasL levels in these samples. We did not detect an increase in murine sFasL levels in sera from SJS/TEN model mice (data not shown). Therefore granulysin was unlikely to be a candidate for mediating conjunctival cell death in SJS/TEN in our model mice.

Development of an SJS/TEN mouse model using PBMCs and the skin of patients who had recovered from SJS/TEN

In our novel SJS/TEN mouse model skin manifestations did not appear; these model mice do not mimic human SJS/TEN completely because the target epithelium was murine in origin. We tried to generate another mouse model to simulate skin manifestations.

First, skin from a patient who had recovered from SJS/TEN was grafted onto the backs of NOG mice. After engraftment was confirmed, PBMCs from the same patient were administered intravenously, followed by oral administration of the causative drug (Fig 3, *A*). In this model both the effector cells and the target cells originate from the same patient with SJS/TEN.

Darkening appeared in the skin graft at 4 days after PBMC injection (Fig 3, *B*). The darkened area increased at 8 days after PBMC injection (Fig 3, *C*). In contrast, we observed no color changes and histologic findings showed few keratinocyte deaths in skin-grafted areas at 8 days after PBMC injection without causative drug intake (see Fig E7 in this article's Online Repository at www.jacionline.org). With PBMCs and skin from the same healthy control subject, no necrotic area appeared. Detection of caspase-3 proves that apoptosis has occurred because it is either partially or totally responsible for the proteolytic cleavage of many key proteins, such as the nuclear enzyme poly (ADPribose) polymerase. Using cleaved caspase-3 staining, we confirmed the increase in keratinocyte death in the SJS/TEN skin graft compared with that seen in the healthy control animals (Fig 3, *D*). In addition, we transplanted skin from patients with ODSRs onto NOG mice and injected the same patients' PBMCs, followed by administration of the causative drug or the vehicle. These mice showed no changes in the appearance of the skin-grafted areas. Histopathologically, the number of apoptotic keratinocytes in ODSR model mice did not differ between the causative drug group and the vehicle group (see Fig E8 in this article's Online Repository at www.jacionline.org).

To investigate the infiltrated cell types, we performed skin graft staining. Both human $CD4^+$ and $CD8^+$ T cells were infiltrated in the transplanted skin areas. However, there were no differences in the numbers of cells between the patient with SJS/TEN and the control (Fig 4). These findings indicate that infiltrating lymphocytes are not critical in this model. The manifestations of these models were quite similar to those in skin lesions of patients with SJS/TEN.

DISCUSSION

The present study aimed to develop a mouse model to mimic human SJS/TEN. We succeeded in reproducing SJS/TEN-like manifestations in the mice. Our results provide an SJS/TEN animal model that promises to be useful in experiments involving SJS/TEN.

To date, investigations to reveal the pathomechanism of SJS/TEN have been carried out with human samples. In previous reports reactions in the acute phase of SJS/TEN in peripheral blood and skin lesions were analyzed, and these investigations have shown that inflammatory mediators, proapoptotic mediators, or infiltrated cells in the skin lesions might be linked to the occurrence of SJS/TEN.

Chung et al[10] attempted to identify key molecules in skin lesions (bullae), and they focused on the most highly expressed proapoptotic molecule: granulysin. Granulysin was found to induce cultured keratinocyte death. Furthermore, recombinant granulysin injection into the murine skin elicited skin necrosis. In addition, we detected higher concentrations of serum granulysin in the acute phase of SJS/TEN than in ODSRs.[11] In contrast,

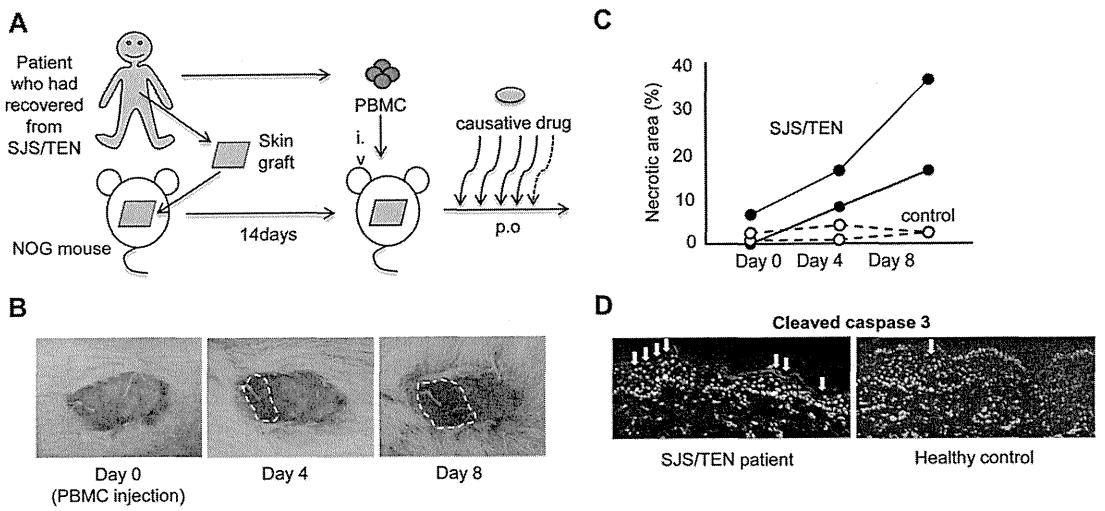

FIG 3. Development of the SJS/TEN mouse model using PBMCs and skin grafts of patients who had recovered from SJS/TEN. **A,** Scheme of mouse model development. Skin grafts from a patient who had recovered from SJS/TEN were grafted onto the backs of NOG mice. After engraftment was confirmed, PBMCs from the same patient were applied intravenously, followed by oral administration of the causative drug. **B** and **C,** Darkened areas appear in the skin graft at 4 days after PBMC injection. These areas were increased at 8 days after PBMC injection. In contrast, the darkened area did not appear in skin grafts of mice when using PBMCs and skin from the healthy control subject. **D,** By using cleaved caspase-3 staining, a great increase in keratinocyte death in the SJS/TEN skin graft was detected in comparison with the keratinocyte death seen in the healthy control specimens. Samples from patient 6 with SJS/TEN and patient 2 with an ODSR were used. *i.v.*, Intravenous; *p.o.*, by mouth.

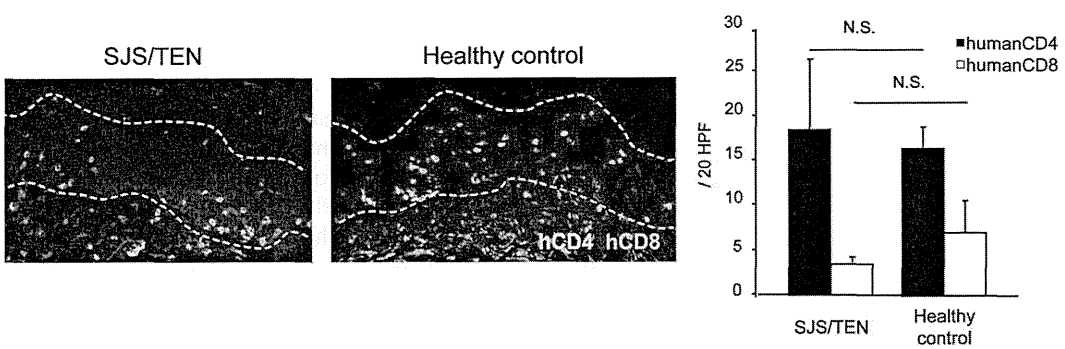

FIG 4. Human CD4 and CD8 staining was performed. Both human $CD4^+$ and $CD8^+$ T cells infiltrated the transplanted skin areas. There were no differences in the numbers of cells between patients with SJS/TEN and controls. Samples from patient 6 with SJS/TEN were used. *HPF,* High-powered field; *N.S.*, not significant.

French's group reported that Fas and Fas ligand interaction is critical in SJS/TEN pathogenesis.[7] They reported that keratinocyte apoptosis in patients with SJS/TEN is mediated by Fas and Fas ligand, which are both expressed on keratinocytes. We also reported that sFasL was able to induce keratinocyte death[8] and that the serum level of sFasL was increased in the acute phase of SJS/TEN, as was the serum level of granulysin.[22] Other candidates, such as α-defensin, have also been reported.[23]

A recent article reported that NK–cytolytic T lymphocyte (CTLs) might be a cell component that contributes to SJS/TEN occurrence. Activated CTLs gain NK cell–like function; these are called NK-CTLs, and they specifically express CD94/NKG2C. NK-CTLs accumulate in skin lesions of patients with SJS/TEN, where they induce keratinocyte death through an interaction between CD94/NKG2C and HLA-E that is expressed specifically on keratinocytes of SJS/TEN lesions.[24]

Even though knowledge regarding the mechanism of SJS/TEN has been accumulated, these findings have never been confirmed in an *in vivo* model. If some molecules were highly expressed in skin lesions or blood during the acute phase of SJS/TEN, there would be no way to confirm whether these molecules are key players. Regarding proapoptotic molecules, several candidates have been reported, as described above. However, most reports focused on molecules that researchers anticipated to contribute to SJS/TEN pathogenesis. Granulysin was identified by means of DNA microarray of cells in bullae; however, not only did the data show that the mRNA level of granulysin was increased, they also showed that the mRNA levels of other proapoptotic molecules, such as Fas ligand, perforin, and granzyme B, were increased.[10] This suggests that several pathways are activated in the apoptotic phenomenon *in vivo*, and there is no solid evidence of an exclusive key player. Animal model experiments involving

depletion or inhibition of specific molecules were essential in proving their uniqueness. Previous experiments with patients' specimens provided fragmentary information on disease etiology. Our model mice open the possibility of recreating the pathologic conditions of SJS/TEN in mice and conducting circumstantial *in vivo* examinations, such as on the benefits of treatments. In our study $CD8^+$ lymphocyte–depleted PBMCs did not produce SJS-like symptoms, strongly demonstrating that $CD8^+$ lymphocytes are necessary to SJS/TEN pathogenesis. Previous reports showed that $CD4^+$ T cells were the predominant population that infiltrated into "maculopapular rash" skin lesions and that most drug-specific T cells were $CD4^+$ T cells.[25] However, in severe cutaneous adverse drug reactions $CD8^+$ T cells were the predominant population that infiltrated into the epidermis of skin lesions of patients with SJS/TEN,[10] and HLA-B*1502 was found to be associated with carbamazepine-induced SJS in all cases.[26] In addition, drug-specific $CD8^+$ T cells were found to predominantly proliferate during the acute stages of SJS.[27] Although drug-specific $CD4^+$ T cells are essential in drug-mediated immune reactions, $CD8^+$ T cells are critical to the development of SJS/TEN. Furthermore, in the skin lesions of model mice, the numbers of $CD4^+$ and $CD8^+$ lymphocytes did not differ between patients with SJS/TEN and control subjects. These findings indicate that infiltrating lymphocytes are not required to generate SJS/TEN skin lesions. Given the findings of ocular lesions, we made the supposition that soluble factors might be involved in keratinocyte death. Although granulysin and sFasL were not specific mediators of this phenomenon, we speculated that causative drug–stimulated PBMCs from patients with SJS/TEN secreted certain cell-death mediators.

Our data using this model also suggest that drug presentation and recognition in the skin might be less necessary than expected because some symptoms develop with little or no recruitment of drug-specific T cells. In our model mice it seems that drug-specific cells were presented and activated by APCs at the spleen and not the skin. Therefore we consider that human APCs presented drug/antigen to T cells in the spleen or peripheral blood. Taken together, we conclude that soluble factors from $CD8^+$ lymphocytes are critical for SJS/TEN development. Our model mice are useful experimental tools to reveal the SJS/TEN pathomechanism.

It is possible that PBMCs from patients with SJS/TEN, which are activated by the causative drug, are highly proliferative and lead to human PBMC reconstitution at day 12, resulting in accelerated GVHRs. However, GVHRs are mediated by human cell infiltration into murine tissue. Indeed, in the GVHR model we detected numerous human cells in the conjunctiva of the mice, whereas in the SJS/TEN-PBMC model, we detected few human cells in conjunctiva and peripheral blood at day 12. These data indicated that at least the ocular manifestations of mice receiving SJS/TEN-PBMC/drug at day 12 were not GVHRs. If PBMCs are highly proliferative at day 12, ocular manifestations can be regarded as a drug-specific phenomenon because mice receiving only PBMCs from patients with SJS/TEN never show such symptoms.

In our model mice it is speculated that the APCs of mice presented drug/antigens to human drug-specific lymphocytes. However the NOG mice used in our experiments have no T, B, and NK cells. In addition, the dendritic cells (DCs) of NOG mice are deficient in antigen presentation.[19] Indeed, dysfunction of DCs allowed engraftment by human cells in NOG mice (ie, DCs of NOG were unable to present xenoantigen to human lymphocytes sufficiently). Therefore we assume that donor human APCs present drug antigens to T cells. Furthermore, by using human IFN-γ ELISpot, the number of drug-specific lymphocytes increased in the spleens of the SJS/TEN-PBMC model mice.

From the clinical aspect, issues have included the difficulty of early diagnosis of SJS/TEN and unresponsiveness to treatment. In the early stage SJS/TEN presents clinically as edematous papules or erythema multiforme–like target rashes that are very similar to those of ODSRs. Such a clinical course makes it difficult to reach a diagnosis of SJS/TEN in the early stage, which results in high mortality rates. Furthermore, the majority of SJS/TEN cases progress rapidly within a few days; therefore methods of early diagnosis are urgently required. We previously analyzed serum samples from 5 patients with SJS/TEN in the early stage (before skin erosions or mucous lesions appeared) and showed that serum levels of sFasL and granulysin are predictors of SJS/TEN diagnosis.[11,22] However, collecting samples at the early stage was quite difficult because of the rarity of the diseases and the intractability of the diagnosis in the early stage, as mentioned above. The present mouse model might allow assessment of changes over time and provide other predictors of early diagnosis and severity of SJS/TEN. Furthermore, treatment interventions are able to be implemented in the early phase in our model, contributing to the prediction of disease onset and prognosis.

We thank Ms Ayumi Moriya for her technical expertise.

Clinical implications: We report a novel mouse model of SJS/TEN that was developed by using PBMCs and skin from patients who had recovered from SJS/TEN. The model promises to promote diagnostic and therapeutic approaches.

REFERENCES

1. Roujeau JC, Kelly JP, Naldi L, Rzany B, Stern RS, Anderson T, et al. Medication use and the risk of Stevens-Johnson syndrome or toxic epidermal necrolysis. N Engl J Med 1995;333:1600-7.
2. Bastuji-Garin S, Rzany B, Stern RS, Shear NH, Naldi L, Roujeau JC. Clinical classification of cases of toxic epidermal necrolysis, Stevens-Johnson syndrome, and erythema multiforme. Arch Dermatol 1993;129:92-6.
3. Di Pascuale MA, Espana EM, Liu DT, Kawakita T, Li W, Gao YY, et al. Correlation of corneal complications with eyelid cicatricial pathologies in patients with Stevens-Johnson syndrome and toxic epidermal necrolysis syndrome. Ophthalmology 2005;112:904-12.
4. Pereira FA, Mudgil AV, Rosmarin DM. Toxic epidermal necrolysis. J Am Acad Dermatol 2007;56:181-200.
5. Schneck J, Fagot JP, Sekula P, Sassolas B, Roujeau JC, Mockenhaupt M. Effects of treatments on the mortality of Stevens-Johnson syndrome and toxic epidermal necrolysis: a retrospective study on patients included in the prospective EuroSCAR Study. J Am Acad Dermatol 2008;58:33-40.
6. Chung WH, Hung SI. Recent advances in the genetics and immunology of Stevens-Johnson syndrome and toxic epidermal necrosis. J Dermatol Sci 2012; 66:190-6.
7. Viard I, Wehrli P, Bullani R, Schneider P, Holler N, Salomon D, et al. Inhibition of toxic epidermal necrolysis by blockade of CD95 with human intravenous immunoglobulin. Science 1998;282:490-3.
8. Abe R, Shimizu T, Shibaki A, Nakamura H, Watanabe H, Shimizu H. Toxic epidermal necrolysis and Stevens-Johnson syndrome are induced by soluble Fas ligand. Am J Pathol 2003;162:1515-20.
9. Posadas SJ, Padial A, Torres MJ, Mayorga C, Leyva L, Sanchez E, et al. Delayed reactions to drugs show levels of perforin, granzyme B, and Fas-L to be related to disease severity. J Allergy Clin Immunol 2002;109:155-61.
10. Chung WH, Hung SI, Yang JY, Su SC, Huang SP, Wei CY, et al. Granulysin is a key mediator for disseminated keratinocyte death in Stevens-Johnson syndrome and toxic epidermal necrolysis. Nat Med 2008;14:1343-50.

11. Abe R, Yoshioka N, Murata J, Fujita Y, Shimizu H. Granulysin as a marker for early diagnosis of the Stevens-Johnson syndrome. Ann Intern Med 2009;151: 514-5.
12. Lee JY, Chae DW, Kim SM, Nam ES, Jang MK, Lee JH, et al. Expression of FasL and perforin/granzyme B mRNA in chronic hepatitis B virus infection. J Viral Hepat 2004;11:130-5.
13. Das H, Imoto S, Murayama T, Kajimoto K, Sugimoto T, Isobe T, et al. Levels of soluble FasL and FasL gene expression during the development of graft-versus-host disease in DLT-treated patients. Br J Haematol 1999;104: 795-800.
14. Azukizawa H, Kosaka H, Sano S, Heath WR, Takahashi I, Gao XH, et al. Induction of T-cell-mediated skin disease specific for antigen transgenically expressed in keratinocytes. Eur J Immunol 2003;33:1879-88.
15. Azukizawa H, Sano S, Kosaka H, Sumikawa Y, Itami S. Prevention of toxic epidermal necrolysis by regulatory T cells. Eur J Immunol 2005;35:1722-30.
16. Nakata H, Maeda K, Miyakawa T, Shibayama S, Matsuo M, Takaoka Y, et al. Potent anti-R5 human immunodeficiency virus type 1 effects of a CCR5 antagonist, AK602/ONO4128/GW873140, in a novel human peripheral blood mononuclear cell nonobese diabetic-SCID, interleukin-2 receptor gamma-chain-knocked-out AIDS mouse model. J Virol 2005;79:2087-96.
17. Beeler A, Engler O, Gerber BO, Pichler WJ. Long-lasting reactivity and high frequency of drug-specific T cells after severe systemic drug hypersensitivity reactions. J Allergy Clin Immunol 2006;117:455-62.
18. Rozieres A, Hennino A, Rodet K, Gutowski MC, Gunera-Saad N, Berard F, et al. Detection and quantification of drug-specific T cells in penicillin allergy. Allergy 2009;64:534-42.
19. Ito M, Hiramatsu H, Kobayashi K, Suzue K, Kawahata M, Hioki K, et al. NOD/SCID/gamma(c)(null) mouse: an excellent recipient mouse model for engraftment of human cells. Blood 2002;100:3175-82.
20. Ito M, Kobayashi K, Nakahata T. NOD/Shi-scid IL2rgamma(null) (NOG) mice more appropriate for humanized mouse models. Curr Top Microbiol Immunol 2008;324:53-76.
21. Ito R, Katano I, Kawai K, Hirata H, Ogura T, Kamisako T, et al. Highly sensitive model for xenogenic GVHD using severe immunodeficient NOG mice. Transplantation 2009;87:1654-8.
22. Murata J, Abe R, Shimizu H. Increased soluble Fas ligand levels in patients with Stevens-Johnson syndrome and toxic epidermal necrolysis preceding skin detachment. J Allergy Clin Immunol 2008;122:992-1000.
23. Morel E, Alvarez L, Cabanas R, Fiandor A, Diaz R, Escamochero S, et al. Expression of alpha-defensin 1-3 in T cells from severe cutaneous drug-induced hypersensitivity reactions. Allergy 2011;66:360-7.
24. Morel E, Escamochero S, Cabanas R, Diaz R, Fiandor A, Bellon T. CD94/NKG2C is a killer effector molecule in patients with Stevens-Johnson syndrome and toxic epidermal necrolysis. J Allergy Clin Immunol 2010;125:703-10, e1-10.
25. Hari Y, Frutig-Schnyder K, Hurni M, Yawalkar N, Zanni MP, Schnyder B, et al. T cell involvement in cutaneous drug eruptions. Clin Exp Allergy 2001;31:1398-408.
26. Chung WH, Hung SI, Hong HS, Hsih MS, Yang LC, Ho HC, et al. Medical genetics: a marker for Stevens-Johnson syndrome. Nature 2004;428:486.
27. Hanafusa T, Azukizawa H, Matsumura S, Katayama I. The predominant drug-specific T-cell population may switch from cytotoxic T cells to regulatory T cells during the course of anticonvulsant-induced hypersensitivity. J Dermatol Sci 2012; 65:213-9.

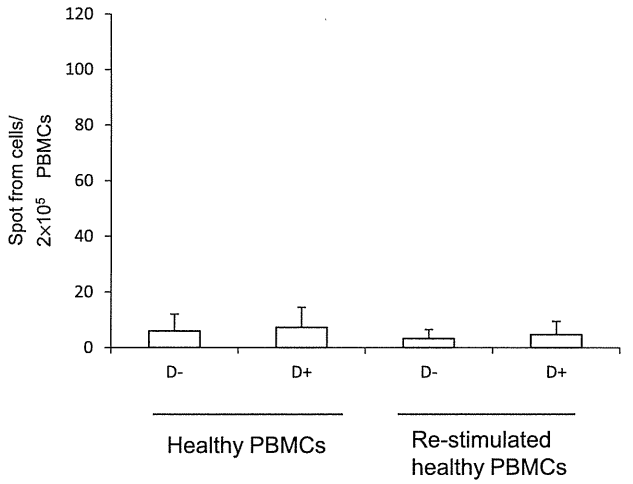

FIG E1. ELISpot assays with PBMCs of naive healthy volunteers who had never experienced cutaneous adverse drug reaction were performed. PBMCs of healthy volunteers (n = 4) were stimulated with amoxicillin, one of the causative drugs in our study, and restimulated after 5 days. ELISpot analysis did not detect drug-specific T cells, even in restimulation. *D+*, Drug addition; *D−*, no drug addition.

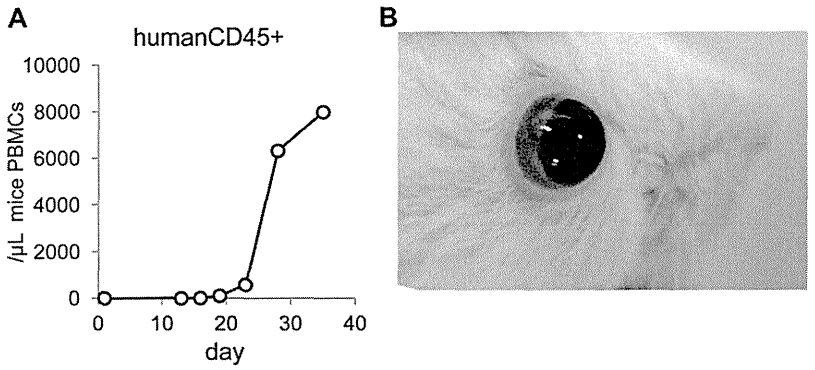

FIG E2. **A,** Human $CD45^{+}$ cells were detected in peripheral blood of NOG mice 20 days after PBMC injection. **B,** Ocular manifestations 14 days after PBMC injection.

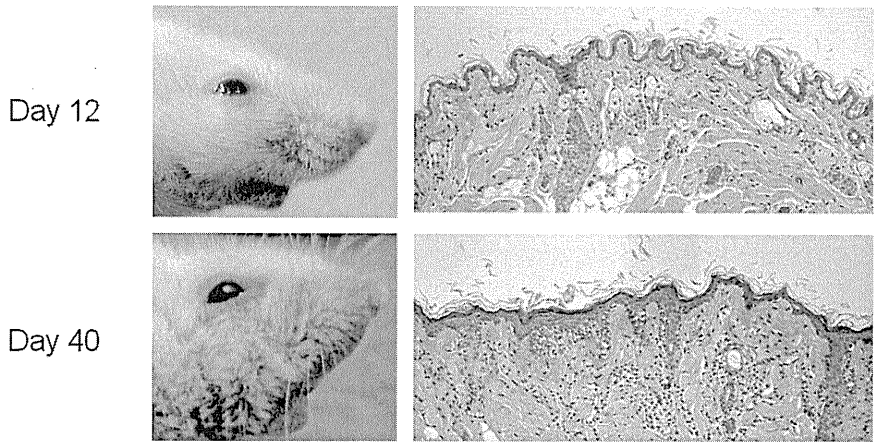

FIG E3. At 12 days after injection of PBMCs from patients with SJS/TEN, NOG mice receiving causative drug showed no significant skin manifestation, and histologic findings indicated intact skin. At 40 days after injection of PBMCs from patients with SJS/TEN, these NOG mice showed weight loss, skin erosion, hair loss, and diarrhea. Prominent epithelial cell death was observed histologically. Samples from patients 1 and 2 with SJS/TEN were analyzed, and representative data (patient 2 with SJS/TEN) are shown.

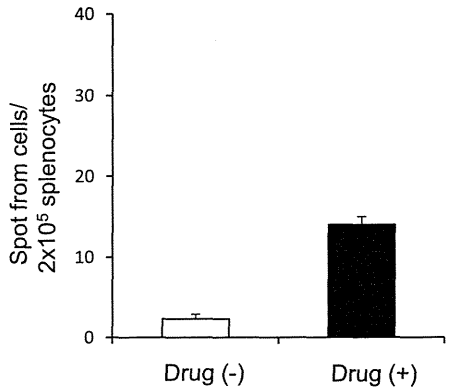

FIG E4. *Increase in drug-specific T-cell numbers in the spleens of NOG mice at 12 days after transfer of PBMCs from patients with ODSRs orally given causative drug is detected by using the ELISpot assay. These results are comparable with those for patients with SJS/TEN. Samples from patient 1 with an ODSR were analyzed.*

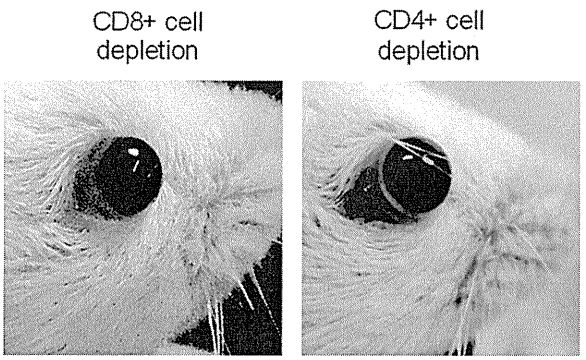

FIG E5. At 12 days after injection of $CD4^+$ T lymphocyte–depleted PBMCs from patients with SJS/TEN and causative drug intake, significant conjunctival congestion and conjunctival chemosis were noticed, whereas this was not the case with $CD8^+$ T lymphocyte–depleted PBMCs from patients with SJS/TEN. Samples from patient 2 with SJS/TEN were analyzed.

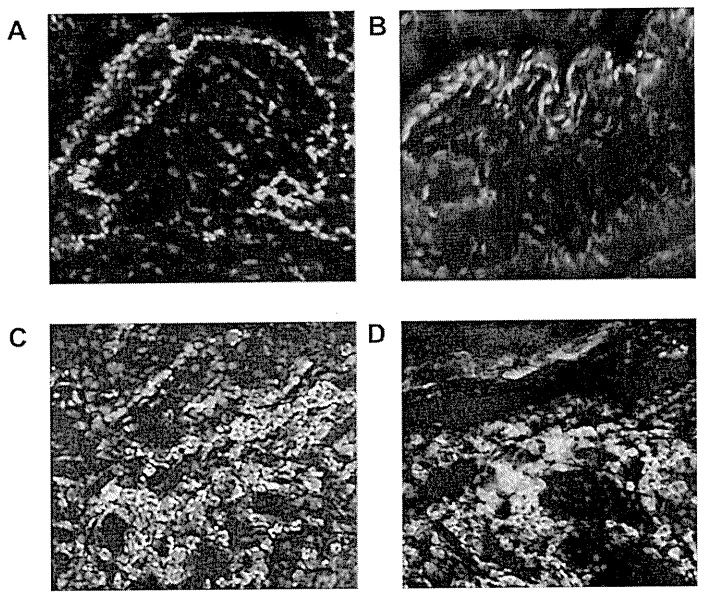

FIG E6. The conjunctiva of SJS/TEN model mice or mice with GVHRs were stained with anti-human CD45 antibodies. FITC-conjugated goat anti-mouse IgG was used as the secondary antibody. The nuclei were counterstained with propidium iodide. **A,** Day 12 for PBMCs from patients with SJS/TEN with causative drug intake. **B,** Day 12 for the GVHD model. **C,** Day 40 for PBMCs from patients with SJS/TEN with causative drug intake. **D,** Day 40 for the GVHD model. In the conjunctiva of both SJS/TEN model and GVHR model mice, there are almost no infiltrating human $CD45^+$ cells at day 12 after PBMC injection, whereas numerous human cells are detected in the conjunctiva of both SJS/TEN model and GVHR model mice. Samples from patients 1 and 2 with SJS/TEN were analyzed, and representative data (patient 2 with SJS/TEN) are shown.

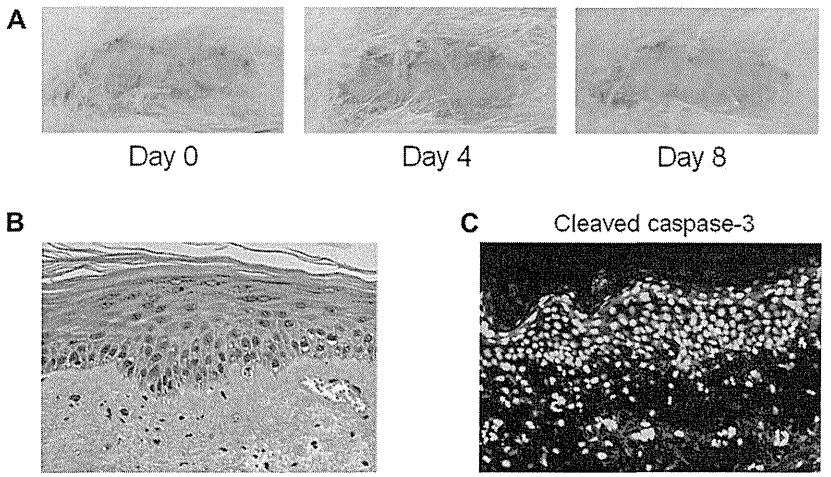

FIG E7. Skin from a patient who had recovered from SJS/TEN was grafted onto the back of NOG mice. After engraftment was confirmed, PBMCs from the same patient were administered intravenously without causative drug administration. Histopathologically, there were few apoptotic keratinocytes in the skin-grafted area. Cleaved caspase-3 staining showed almost no positive cells in the skin-grafted area. Samples from patient 6 with SJS/TEN were analyzed.

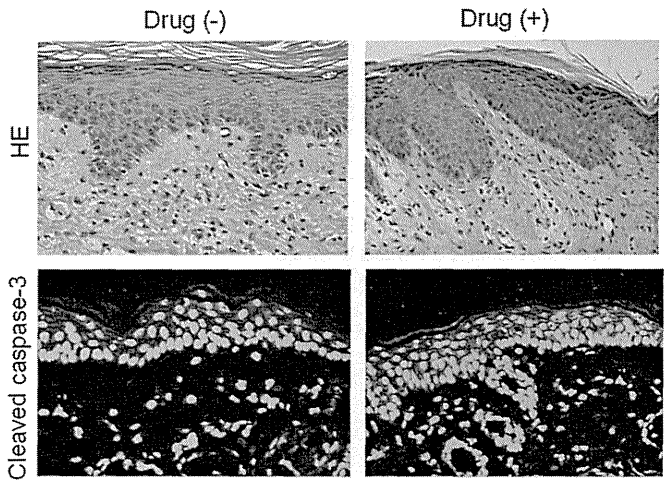

FIG E8. Skin grafts from patients with ODSRs were transplanted onto NOG mice, which were then injected with PBMCs from the same patients, followed by the causative drug or vehicle. These mice showed no changes in appearance of the skin-grafted areas. Histopathologically, there were few *dead keratinocytes and few cleaved caspase-3–positive cells in the skin* graft. Samples from patient 2 with ODSR were analyzed. *HE,* Hematoxylin and eosin.

TABLE E1. Patient information

Case	Age (y)/sex	Causative drug	Type of cADR	SI
SJS/TEN				
1	55/M	Acetaminophen	TEN	2.4
2	46/M	Acetaminophen	SJS	2.0
3	49/F	Acetaminophen	SJS	2.3
4	49/M	Benzbromarone	SJS	2.9
5	37/F	Amoxicillin	SJS	2.0
6	71/M	Phenytoin	SJS	2.5
ODSR				
1	70/M	Acetaminophen	Maculopapular	2.0
2	78/M	Phenytoin	Maculopapular	6.7

cADR, Cutaneous adverse drug reaction; *F*, female; *M*, male; *SI*, stimulation index.

Journal of Dermatological Science xxx (2013) xxx–xxx

Contents lists available at SciVerse ScienceDirect

Journal of Dermatological Science

journal homepage: www.elsevier.com/jds

Establishment of a novel experimental model of human angiosarcoma and a VEGF-targeting therapeutic experiment

Daichi Hoshina, Riichiro Abe *, Naoya Yoshioka, Nao Saito, Hiroo Hata, Yasuyuki Fujita, Satoru Aoyagi, Hiroshi Shimizu *

Department of Dermatology, Hokkaido University Graduate School of Medicine, Sapporo, Japan

ARTICLE INFO

Article history:
Received 6 October 2012
Received in revised form 1 February 2013
Accepted 20 February 2013

Keywords:
Angiosarcoma
VEGF
Bevacizumab
Sunitinib

ABSTRACT

Background: Angiosarcoma is one of the most life-threatening neoplasms with strong resistance to conventional chemotherapy/radiotherapy; consequently, alternative therapeutic agents are urgently required. One factor in delaying the therapy development is the limitation of experimental models.
Objective: We established a novel experimental angiosarcoma model.
Methods: From surgically resected tissue, human AS cell line was established. Using xenograft of AS cell line, we performed therapeutic experiments with the anti-human VEGF Ab or the receptor tyrosine kinase inhibitor.
Results: First we generated an angiosarcoma cell line, HAMON (human angiosarcoma, monoclonal), which expresses CD31 and produces tumors in immunodeficient mice. HAMON expresses VEGFR2 and that exogenous VEGF leads to HAMON proliferation *in vitro*. Anti-human VEGF Ab bevacizumab treatment failed to suppress HAMON proliferation *in vitro* and *in vivo*. Furthermore, the receptor tyrosine kinase inhibitor sunitinib did not suppress HAMON proliferation *in vitro*. Similarly, in *in vivo* therapeutic experiments, even high doses of sunitinib failed to inhibit tumor growth. Finally, we checked whether compensatory activation of VEGF signaling occurred after sunitinib addition. VEGF protein secretion, VEGF mRNA synthesis and VEGFR2 phosphorylation all were unaffected in HAMON after sunitinib treatment.
Conclusion: A novel *in vitro* and *in vivo* experimental model of human angiosarcoma has been successfully established. With this model, we were able to perform therapeutic experiments. In addition, our angiosarcoma cell line, HAMON, is quite useful for identifying key molecules in angiosarcoma.

1. Introduction

Angiosarcoma (AS) is one of the most aggressive mesenchymal tumors and has a relatively rare incidence (2% of soft tissue sarcomas) [1]. While AS can occur in any organ, the most commonly affected organ is the skin, especially the scalp and face of elderly people [2]. Although radiation and chemotherapy are the preferred therapies, recurrence and metastasis frequently occurs. The prognosis remains poor, and the overall 5-year survival rate is approximately 35% [3]. The most optimistic survey suggests that only 60% of patients survive for more than 5 years, with a median survival of 7 months [4].

AS biology has not been fully clarified because experimental models of human AS have been quite limited. Only two AS cell lines, ISO-HAS [5] and AS-M [6], have been reported, and almost no therapeutic experiments with a relevant *in vivo* model of human AS have been performed, which has delayed the establishment of efficient therapies for human AS.

VEGF is the most potent angiogenic factor; it is known to be up-regulated in several malignant tumors, and it has been regarded as playing the most important role in tumor angiogenesis and consequent tumor survival [7]. On the assumption that the blockage of tumor neovascularization leads to the inhibition of tumor growth, several VEGF signaling-targeted agents have been developed and have shown significant anti-tumor efficacy, even against advanced-stage tumors [8].

E-mail address: aberi@med.hokudai.ac.jp.
* Corresponding authors at: Department of Dermatology, Hokkaido University Graduate School of Medicine, N15 W7, Sapporo 060-8638, Japan.
Tel.: +81 11 706 7387; fax: +81 11 706 7820.

0923-1811/$36.00
http://dx.doi.org/10.1016/j.jdermsci.2013.02.008

Please cite this article in press as: Hoshina D, et al. Establishment of a novel experimental model of human angiosarcoma and a VEGF-targeting therapeutic experiment. J Dermatol Sci (2013), http://dx.doi.org/10.1016/j.jdermsci.2013.02.008

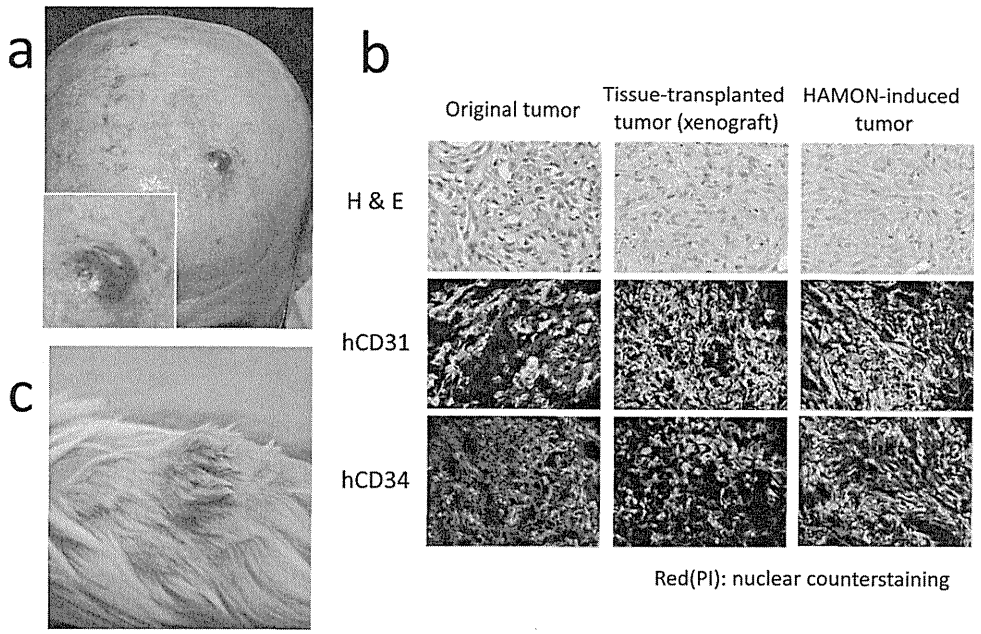

Fig. 1. (a) Clinical appearance of original AS tumor. (b) Hematoxylin and eosin staining and immunofluorescence. Histopathological findings were preserved for the primary AS tumor, xenografted tumor and HAMON tumor. Original magnification 400×. (c) Appearance of xenografted tumor on NOD/*Scid* mouse.

AS is considered to be an endothelial cell-originating soft-tissue sarcoma, and VEGF is assumed to be strongly associated with AS biological behavior [9]. Recent studies have demonstrated that AS expresses VEGF and VEGF receptors (VEGFRs), and AS is thought to be dependent on VEGF signaling for proliferation, invasion and metastasis [10,11]. Therefore, drugs targeting VEGF signaling seem promising as novel therapeutic agents against AS.

Here, we report a novel *in vitro* and *in vivo* experimental model of human AS. With this model, we performed therapeutic experiments with the anti-human VEGF antibody bevacizumab and with the receptor tyrosine kinase inhibitor sunitinib. From the outcome of the therapeutic experiments, we investigated VEGF signaling in AS.

2. Materials and methods

2.1. AS tissue sampling and the development of the AS xenograft

AS tissue was taken from a recurrent tumor on the scalp of an 81-year-old Japanese male (Fig. 1a). The patient received radiation therapy prior to resection of the tumor. A 5-mm × 5-mm × 5-mm piece of AS tissue was subcutaneously transplanted with matrigel (BD Bioscience, Franklin Lakes, NJ, USA) onto the flank of a 4–5-month-old female NOD/*Scid* mouse (Clea, Tokyo, Japan). The medical ethics committee of Hokkaido University approved all the described studies. Animal use procedures were approved by the institutional committee of the Hokkaido University Graduate School of Medicine.

2.2. Establishment of the cell line

Tumor tissue of xenografted mice was minced and digested with collagenase (Roche, Basel, Switzerland) at 37 °C overnight. The digested tissue was filtered through a 115-μm mesh. After centrifugation, the pellets were seeded in a medium for endothelial cells (EBM-2: Clonthec, Mountain View, CA, USA) on collagen-coated dishes (Iwaki, Tokyo, Japan). To achieve a stable cell culture, several growth factors were added to the medium, including hydrocortisone, VEGF, ascorbic acid, basic-fibroblast growth factore (bFGF), insulin-like growth factor-1 (IGF-1), epidermal growth factor (EGF), heparin and FBS. After stable cell proliferation was achieved, limited dilution subcloning was performed. Except as noted, all experiments were done with this established cell line.

*2.3. Re-transplantation of the AS cell line into NOD/*Scid *mice*

The AS cell line (3×10^6 cells) were injected with matrigel (BD, Franklin Lakes, NJ, USA) into the flank of NOD/*Scid* mice. Two months after transplantation, the tumor was excised and HE staining and immunofluorescence was performed with the aforementioned antibodies.

2.4. In vitro *tube formation assay*

An *in vitro* angiogenesis assay kit (Chimicon, Billerica, MA, USA) was used for evaluation of the tube formation ability of the AS cell line according to the manufacturer's instructions. Briefly, after 1 h of incubation of matrix solution transferred to a pre-cooled 96-well culture plate, 1×10^4 cells were seeded onto the surface of the matrix. Tube formation was assayed 7 and 22 h after seeding. As a control, human umbilical vein endothelial cells (HUVEC cells, Takara Bio, Shiga, Japan) were also evaluated.

2.5. Flow cytometry and western blotting for VEGFR2

A suspension of AS cells and HUVEC was stained by mouse anti-human CD31 monoclonal Ab or mouse anti-human VEGFR2 monoclonal Ab (Abcam, Cambridge, MA, USA) as the primary Abs, and FITC-conjugated goat anti-mouse polyclonal Ab (Jackson, Bar Harbor, ME, USA) as the secondary Ab. Analysis was performed using FACS-Aria with BD FACSDiVa software (BD Biosciences).

For western blotting, cell lysate was extracted with Cell Lysis Buffer (Cell Signaling Technology, Danvers, MA, USA). Rabbit anti-human VEGFR2 Ab (Cell Signaling Technology) was used as the primary Ab. The western blotting protocol followed the manufacturer's instructions.

Please cite this article in press as: Hoshina D, et al. Establishment of a novel experimental model of human angiosarcoma and a VEGF-targeting therapeutic experiment. J Dermatol Sci (2013), http://dx.doi.org/10.1016/j.jdermsci.2013.02.008

2.6. In vitro *proliferation assay with exogenous VEGF and inhibitory assay*

Cells were seeded onto a collagen-coated 96-well plate (Iwaki) (1×10^4 per well) in EBM-2 and allowed to attach. After confirming cell attaching, the medium was changed to the one without VEGF. After 16 h of starvation, 50 ng/ml recombinant VEGF (Sigma, St. Louis, MO, USA) was added. After 4 days, cell proliferation was evaluated using Cell Proliferation ELISA, BrdU (Roche) according to the manufacturer's instructions. Absorbance was measured at 490 nm using Mithras LB940 (Berthold, Tokyo, Japan).

As an inhibitory assay, bevacizumab (provided by Chugai Pharmaceutical, Tokyo, Japan) or sunitinib (LC Laboratories, Woburn, MA, USA) was added in several concentrations 1 day after cell seeding. After 4 days, cell viability was evaluated using Cell Proliferation ELISA, BrdU. Experiments were done in quintuple and repeated at least three times.

2.7. In vivo *therapeutic experiments*

NOD/*Scid* mice (4–6 wk old) were implanted subcutaneously with a 5-mm × 5-mm × 5-mm piece of human AS tissue that had been serially transplanted and maintained on another NOD/*Scid* mice. After tumors grew to about 200 mm^3, drug administration was started. As for bevacizumab, 5 mg/kg/week or 10 mg/kg/week was intraperitoneally administered weekly for 7 weeks. As for sunitnib, 40 mg/kg/day or 120 mg/kg/day sunitinib diluted with 200 μl citrate buffer was orally administered daily for 2 weeks. To calculate the tumor volume, we utilized the following formula: (long axis) × (short axis)^2/2 (mm^3).

2.8. *Quantitative real-time PCR analysis for VEGF*

The transition of VEGF mRNA synthesis after VEGFR2 blocking with sunitinib was evaluated. Based on the results of the inhibitory assay, 100 nM sunitinib was added to 1×10^6 culture cells. Thirty minutes after sunitinib addition, PBS wash was performed and RNA was extracted using the RNeasy Mini Kit (Qiagen, Valencia, CA, USA). Real-time PCR was performed with the ABI Prism 7000 Sequence Detection System (Applied Biosystems, Carlsbad, CA, USA) using commercially available TaqMan Gene Expression Assays (Applied Biosystems) of VEGF (Hs00900055_m1) and GAPDH Endogenous Control (4326317E), and TaqMan Gene Expression Master Mix (Applied Biosystems) according to the manufacturer's instructions.

2.9. *Evaluation of compensatory VEGF secretion and VEGFR2 phosphorylation after sunitinib addition*

The change of VEGF protein secretion and of the VEGFR2 phosphorylation after sunitinib addition was assayed. For VEGF protein secretion, 100 nM sunitinib was added to 2×10^5 culture cells. From 1 to 24 h after sunitinib addition, culture supernatant was taken and VEGF protein concentration was assayed with Quantikine Human VEGF (Roche). Similarly, for VEGFR2 phosphorylation, from 5 to 120 min after 100 nM sunitinib addition, the cell lysate was evaluated with the PathScan Phospho-VEGFR2 (Tyr1175) Sandwich ELISA Kit (Cell Signaling). Absorbance in both assays was measured at 490 nm using Mithras LB940 (Berthold, Japan).

2.10. *Receptor tyrosine kinases array*

The Human Phospho-RTK Array Kit (R&D Systems) and PathScan RTK Signaling Antibody Array Kit (Cell Signal Technology) were used according to the manufacturer's protocols. Seventy-five micrograms of whole-cell lysate were applied to each array; after western blotting, films were scanned for densitometric analysis using ImageJ Software to determine the percent control activation using equations accounting for lot variation for array strips and background.

2.11. *Statistics*

Statistical analyses for most of the experiments were by *t*-test. $p < 0.05$ was considered to be statistically significant. The data are presented as mean + SE of the indicated number of independent experiments.

3. Results

3.1. *Establishment of the novel human AS cell line HAMON*

To establish a novel human AS cell line, surgically resected tissue was digested and cultured. Alongside the cell culturing, AS tumor tissue was implanted into the flank of NOD/*Scid* mice. The original AS tumor expressed human CD31 and human CD34 (Fig. 1b). Although the cell culture from human AS tissue failed, the implanted AS tumor tissue grew into a dark reddish, easily bleeding tumor over the course of 6 months (Fig. 1c). Histopathological examination demonstrated that the tumor consisted of various-sized immature vessels, compatible with the characteristics of AS (Fig. 1b). Immunofluorescence staining revealed that the tumor cells expressed human CD31 and human CD34 (Fig. 1b).

Cell culturing was re-tried with digested tissue of the implanted tumor and was successfully established. Cultured cells were spindle-shaped, and they proliferated after several passages. Flow cytometric analysis showed the expression of human CD31 and human VEGFR2 (Fig. 2a). Tube formation assay was done for confirming the angiogenic potency of the cultured cells. This assay demonstrated the formation of immature vessel-like structures that were similar to the vessel formation of HMVEC (Fig. 2b). Moreover, subcutaneous injection of cultured cells produced reddish tumor tissue in NOD/*Scid* mice. Histopathological examination of the tissue demonstrated the characteristics of human AS, as confirmed by HE staining and immunofluorescence staining of human CD31 and human CD34 (Fig. 1b). In addition, single-cell cloning was performed using a limited dilution technique and the successfully established cell line was named human angiosarcoma, monoclonal (HAMON).

3.2. *VEGF signaling in HAMON*

AS is regarded as a mesenchymal tumor of endothelial cell origin; thus, it is strongly suspected that a biological nature similar to that of endothelial cells underlies AS. It is well known that VEGF signaling is the greatest factor in promoting angiogenesis; therefore, it was hypothesized that VEGF signaling is critical in AS. HAMON expressed VEGFR2 as well as HMVEC did (Fig. 2c). In contrast, HAMON did not express VEGFR1 (Supplementary Fig. 1). Next, HAMON proliferation assay with exogenous VEGF was performed. Exogenous recombinant VEGF was found to lead to significant HAMON proliferation ($p < 0.05$) (Fig. 2d). These data indicate that the HAMON proliferation was affected by VEGF stimulation.

3.3. *Effect of VEGF blocking with bevacizumab on HAMON proliferation in* in vitro *and on AS tumor* in in vivo

Immunofluorescence revealed HAMON expressed not only VEGFR2 but also VEGF (Fig. 3a). In addition to the result of previous

Please cite this article in press as: Hoshina D, et al. Establishment of a novel experimental model of human angiosarcoma and a VEGF-targeting therapeutic experiment. J Dermatol Sci (2013), http://dx.doi.org/10.1016/j.jdermsci.2013.02.008

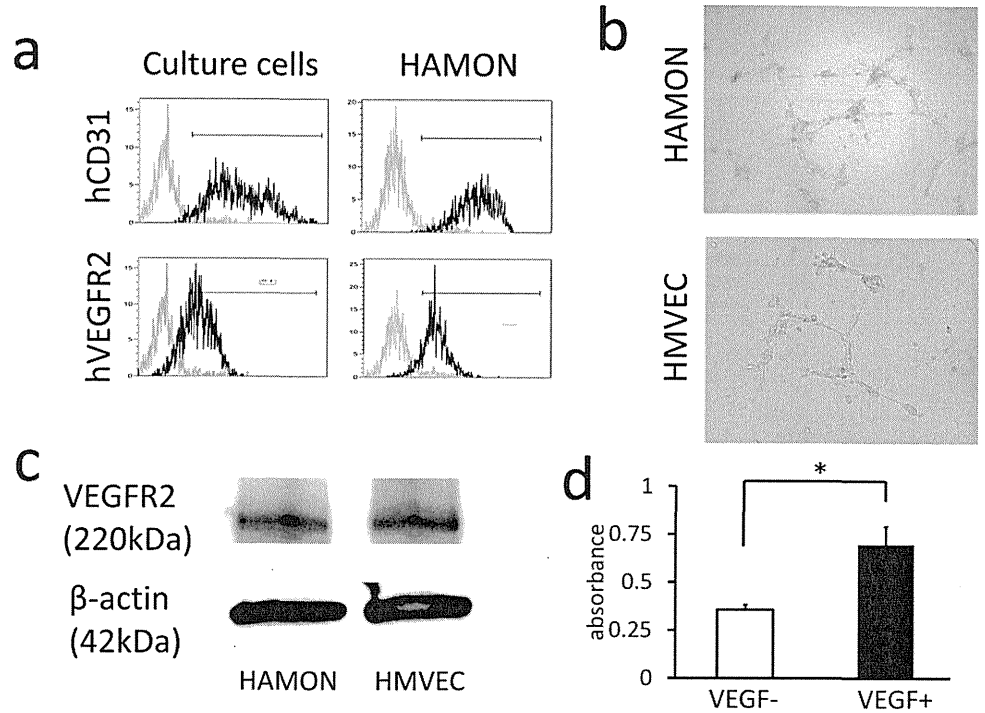

Fig. 2. (a) Flow cytometric analysis of culture cells and HAMON for human CD31 and human VEGFR2. Negative control is shown by light-gray line. (b) Cultured cells form an immature vessel-like structure in *in vitro* tube formation assay. HMVEC was used as a control. (c) Western blotting for human VEGFR2. Cell extract of HMVEC was used as a control. (d) Proliferation assay of HAMON (BrdU ELISA). Exogenous VEGF has accelerated the HAMON proliferation. $^{*}p < 0.05$.

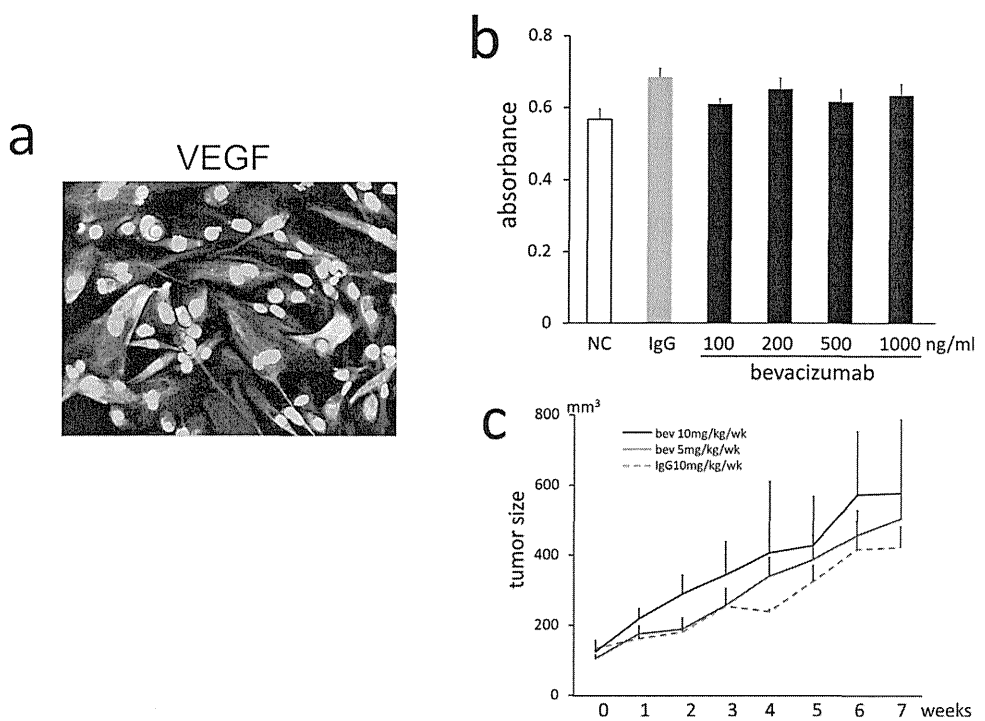

Fig. 3. (a) Immunofluorescence staining for VEGF was performed. HAMON expressed human VEGE in cytoplasm. (b) Cell proliferation assay (BrdU ELISA) showed bevacizumab did not inhibit HAMON proliferation. (c) *In vivo* therapeutic experiments with bevacizumab. Five or 10 mg/kg bevacizumab was administered intraperitoneally weekly for 7 weeks. Neither group of bevacizumab treatments notably suppressed AS tumor growth.

assay with exogeneous VEGF stimulation, these data suggested that autocrined VEGF functions in AS biology. Therefore, the blocking of VEGF with anti-VEGF antibody seemed promising, and we performed *in vitro* inhibitory assay with bevacizumab. However, even 1000 ng/ml bevacizumab did not show remarkable inhibitory effect against HAMON proliferation (Fig. 3b).

Through the outcomes of previous studies [12], it has been considered that bevacizumab monotherapy does not suppress tumor growth. Similarly, in our experiment, even 10 mg/kg/week bevacizumab did not affect AS tumor growth and survival duration in NOD/*Scid* mice (Fig. 3c). In addition, there was no significant difference in the expression level of the hypoxic marker

Please cite this article in press as: Hoshina D, et al. Establishment of a novel experimental model of human angiosarcoma and a VEGF-targeting therapeutic experiment. J Dermatol Sci (2013), http://dx.doi.org/10.1016/j.jdermsci.2013.02.008

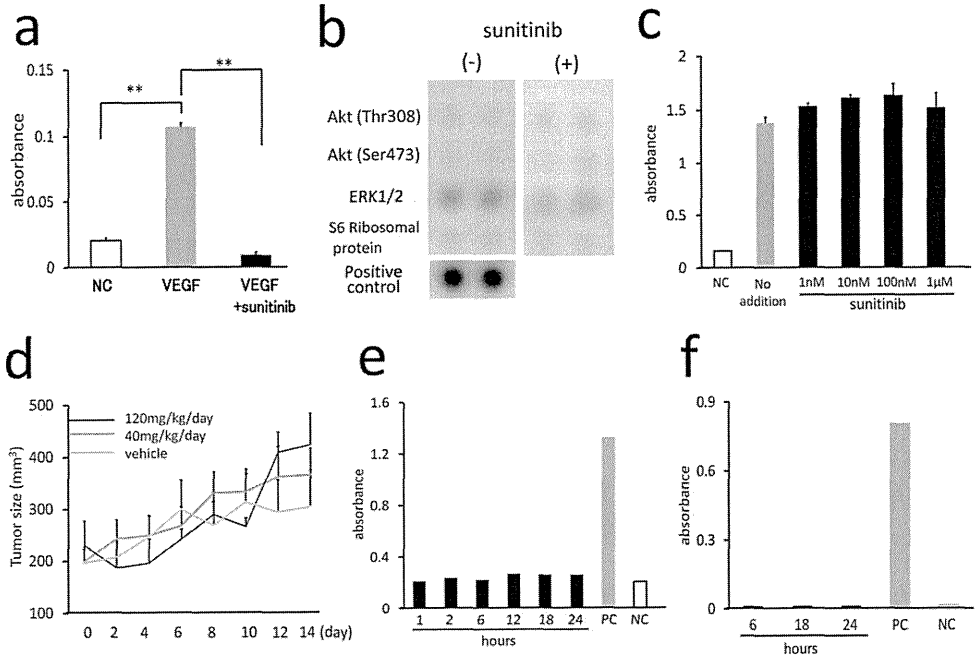

Fig. 4. *Sunitinib treatment and VEGF signaling in HAMON.* (a) ELISA for VEGFR2 phosphorylation. Whereas exogenous VEGF has promoted VEGFR2 phosphorylation of HAMON, sunitinib has blocked this phosphorylation completely. $^{**}p < 0.01$. (b) Lysates from HAMON treated with or without sunitinib (100 nM) for 10 min were subjected to RTK profiling. In each array, each RTK is assayed in duplicate. (c) Cell proliferation assay (BrdU ELISA). Sunitinib did not inhibit HAMON proliferation. (d) *In vivo* therapeutic experiments with sunitinib. 40 mg/kg/day or 120 mg/kg/day was orally administered daily for 2 weeks. Both groups of sunitinib treatment did not remarkably suppress AS tumor growth. (e) VEGF ELISA under sunitinib exposure. Cell culture supernatants from 0 to 120 min after 10 nM sunitinib addition were assayed. (f) ELISA for VEGFR2 phosphorylation under sunitinib exposure. Transition from 6 to 24 h is shown. Representative data are shown.

pimonidazole between bevacizumab-treated and untreated tumors (Supplementary Fig. 2). These results indicate that VEGF-targeting drugs do not induce hypoxia within angiosarcoma tumors. Therefore, it seems unlikely that there would be hypoxia-induced endothelial cell survival in angiosarcoma tumors with VEGF-targeting monotherapy.

3.4. *Effect of VEGFR blocking with sunitinib on HAMON proliferation* in vitro

First, in order to confirm the efficacy of sunitinib for inhibiting VEGF signaling, VEGFR2 phosphorylation of HAMON was evaluated with and without sunitinib. Whereas exogenous VEGF promoted VEGFR2 phosphorylation of HAMON, sunitinib blocked this promotion completely ($p < 0.01$) (Fig. 4a). This result revealed that sunitinib inhibited VEGFR2 phosphorylation on HAMON. Then we analyzed whether signal transduction pathways downstream of VEGFR2 are activated in HAMON. As a result, a mild degree of ERK1/2 phosphorylation was observed in HAMON constitutively in contrast to other kinase such as Akt (Fig. 4b), and sunitinib inhibited phosphorylation of ERK1/2 (50.5% reduction) (Fig. 4b).

Next, the inhibitory effect of sunitinib on HAMON proliferation was examined. *In vitro* antitumor activity of sunitinib was initially well studied by Mendel et al. [13]. According to their observations, sunitinib inhibited VEGF-induced VEGFR2 tyrosine phosphorylation with IC_{50} values of ~10 nM and cell proliferation of HUVECs with IC_{50} values of 4 nM. However, unexpectedly, even 1 μM sunitinib did not lead to the suppression of HAMON proliferation. In fact, around 100 nM sunitinib seemed to accelerate HAMON proliferation (Fig. 4c). In summary, sunitinib did not inhibit HAMON proliferation.

3.5. *No inhibitory effect of sunitinib on* in vivo *AS tumor growth*

Next, we investigated the therapeutic effect of sunitinib on AS growth in *in vivo*. In previous experiments, the duration of sunitinib treatment in *in vivo* experiments with xenograft mice ranged from 7 days to 74 days, and the administered sunitinib dosage varied from 20 to 120 mg/kg/day [13–15]. Recently, in preclinical therapeutic experiments on neuroblastoma, 20, 30 and 40 mg/kg/day sunitinib were orally administered to neuroblastoma xenograft mice for 2 weeks [15]. In light of these previous experiments, we administered 40 mg/kg/day and 120 mg/kg/day sunitinib orally daily for 2 weeks to human-AS-bearing NOD/*Scid* mice. Forty mg/kg/day sunitinib did not influence the growth of xenografted AS tumors. Similarly, 120 mg/kg/day sunitinib did not remarkably suppress AS tumor growth, and the final volume of AS tumor in the high-dose group was larger than that in the vehicle group ($p = 0.17$) (Fig. 4d). Among the three groups, there was no difference in survival duration. These results indicate that sunitinib did not suppress AS tumor growth. In addition, there was no significant difference in expression level of the hypoxic marker pimonidazole between sunitinib-treated and untreated tumors (Supplementary Fig. 2).

3.6. *No compensatory activation of VEGF signaling in AS through a negative feedback loop*

It has been demonstrated that endothelial cells secrete VEGF by themselves and the VEGF-autocrine pathway is also functional in such cells [16]. This leads us to predict that similar autocrine regulation of VEGF signaling works in AS and that blocking of VEGFR2 by sunitinib leads to a compensatory increase in VEGF transcription or synthesis through a negative feedback loop that might cause *in vitro* and *in vivo* sunitinib therapeutic experiments to fail. Therefore, transitional evaluations of VEGF and VEGFR2 phosphorylation under sunitinib addition were performed. However, compensatory increases in VEGF protein secretion were not observed (Fig. 4e). Similarly, compensatory increases in VEGF mRNA were not found (data not shown). Additionally, the level of VEGFR2 phosphorylation was not altered by sunitinib (Fig. 4f). These results suggest that VEGFR2 blocking with sunitinib does not cause

Please cite this article in press as: Hoshina D, et al. Establishment of a novel experimental model of human angiosarcoma and a VEGF-targeting therapeutic experiment. J Dermatol Sci (2013), http://dx.doi.org/10.1016/j.jdermsci.2013.02.008